

Impurities and Landau level mixing in a fractional quantum Hall state in a flatband lattice model

Topi Siro, Mikko Ervasti, and Ari Harju

COMP Centre of Excellence, Department of Applied Physics, Aalto University, Helsinki, Finland

(Dated: April 4, 2024)

We study the topological checkerboard lattice model around the $\nu = \frac{1}{3}$ fractional quantum Hall phase using numerical exact diagonalization without Landau level projections. We add local perturbations, modified hoppings and on-site potentials, and observe phase transitions from the fractional quantum Hall phase to metallic and insulating phases when the strength and number of impurities is increased. In addition to evaluating the energy spectrum, we identify the phase diagrams by computing the topological Chern number of the many-body ground state manifold, and we show how the ground states lose their correlations due to the impurities by evaluating the spectrum of the one-body reduced density matrix. Our results show that the phase transition from the fractional quantum Hall phase to the metallic phase occurs for both impurity hoppings and potentials. Strong impurity hoppings cause a further transition into the insulating state, regardless of the sign of the hopping, when their density is high enough. In contrast, the same happens only for attractive potentials. Furthermore, the mixing to the higher band in a two-band model, generally denoted as Landau level mixing, is measured concluding that the lowest Landau level projection works well even with remarkably strong interactions and in the presence of impurities.

I. INTRODUCTION

There has been great interest recently in topological lattice models that support states analogous to the ones in the integer and the fractional quantum Hall (FQH) effects^{1,2}. Since the Haldane honeycomb³ model, various topological lattice models have been introduced, most notably ones without a net external magnetic field and with flat energy bands arising from realistic hopping parameters^{4–10}. In these systems the time-reversal invariance is broken to achieve quantized non-zero Hall conductivity, characterized by the non-zero band Chern number¹¹. It has been shown that filling such topological bands according to the standard $\nu = \frac{1}{3}$ and $\nu = \frac{1}{5}$ filling fractions, certain interactions stabilize the FQH phase¹².

The FQH states are robust against weak local perturbations due to the large energy gap between the ground states and the excited states, and due to the topological order present in the ground states induced by the interactions. Therefore, weak disorder should not break the FQH phase. However, when increasing the number and strength of the local impurities, at some point the system becomes a normal metal or an insulator¹³. This has been studied in a topological lattice model with impurity on-site potentials positioned in a single line, showing quantum phase transitions from FQH phase to a metallic phase and with even stronger impurities to an insulating phase¹⁴. However, it is not yet well understood how the positioning of the impurities, and the types of impurities affect the phase diagram. The impurities also change the effective filling fraction of the rest of the system, which could have a pronounced effect to break the FQH phase in finite systems.

The FQH topological phases can be characterized by the topological ground state degeneracy¹⁵, and furthermore by the quasiparticle properties^{2,16,17}. In principle, impurities attract or repel the quasiparticles. One can

even hope to braid quasiparticles by moving the impurities, which has been explicitly done in a numerical simulations of bosonic models^{18,19}. Therefore, it is also interesting to study the effect of individual impurities, especially by observing the changes in the ground states as a function of the impurity strength.

In this work, we study the effect of impurities on the two-band topological checkerboard lattice model around the $\nu = \frac{1}{3}$ FQH phase¹². We consider a variable number of impurities, local perturbations on the nearest-neighbor hoppings, and on-site potentials, with increasing and decreasing values. The impurities are distributed as far away from each other as possible. This setup makes it possible to study two kinds of disorder effects, by keeping the number, or alternatively, the strengths of the impurities fixed, while modifying the other. The quantum phase diagrams are deduced by evaluating the energy spectrum, topological degeneracy, the many-body ground state manifold Chern number, and the spectrum of the one-body reduced density matrix (1-RDM).

The systems are solved using numerical exact diagonalization method in the full state space. This allows us to measure how much the two non-interacting bands mix in the interacting system, generally denoted as Landau level mixing. Due to memory constraints of the exact diagonalization method, we are only able to study quite small finite systems. However, as shown by previous studies^{12,14}, interesting topological features can be observed despite the finite size of the lattice. The results for these small systems are also interesting from the point of view of the potential experimental realizations of flatband lattice models with ultracold atoms in optical lattices.

II. MODEL AND METHODS

The two-band model on a checkerboard lattice was introduced in Ref. 6. The Hamiltonian reads

$$H_0 = \sum_{\langle j,k \rangle} t_{jk} e^{i\phi_{jk}} c_j^\dagger c_k + \sum_{\langle\langle j,k \rangle\rangle} t'_{jk} c_j^\dagger c_k + \sum_{\langle\langle\langle j,k \rangle\rangle\rangle} t''_{jk} c_j^\dagger c_k + \text{H.c.}, \quad (1)$$

where c_j^\dagger and c_j are the fermionic creation and annihilation operators for site j . The sums run over the nearest-neighbor, next-nearest-neighbor and next-next-nearest-neighbor sites, respectively, and the corresponding hopping amplitudes are t , t' , and t'' . The sign of the phase factor ϕ_{jk} alternates between sites as seen in Figure 1. The lowest band is almost flat and has a unit Chern number. To minimize the dispersion in the lowest band, we use the values given in Ref. 6: $\phi_{jk} = \pi/4$, $t = 1$, $t' = \pm 1/(2 + \sqrt{2})$ and $t'' = 1/(2 + 2\sqrt{2})$. Note that we have reversed the sign of the Hamiltonian in Ref. 6 to make the flat band lowest in energy.

To obtain the $\nu = \frac{1}{3}$ FQH state, we add a nearest-neighbor repulsive interaction,

$$H = H_0 + V \sum_{\langle j,k \rangle} n_j n_k, \quad (2)$$

where $n_j = c_j^\dagger c_j$ counts the number of electrons at site j . In Ref. 12 it was shown that for suitable values of V , there is a threefold quasi-degenerate ground state manifold (GSM), separated from the higher states by a large gap. We introduce twisted boundary conditions,

$$\psi(x_j + L_j) = e^{i\theta_j} \psi(x_j), \quad (3)$$

where j indexes the space dimensions and L_j is the length of the system along direction j . The gap above the GSM remains open for all values of θ_1 and θ_2 , and the ground state manifold has a Chern number equal to ± 1 , indicating a topological FQH phase. The Chern number is a topological invariant, defined as the integral of the Berry curvature over the (θ_1, θ_2) plane. In practice, we calculate the Berry curvature by dividing the (θ_1, θ_2) plane into a discrete lattice of $N_\theta \times N_\theta$ points. At each point, the Berry curvature is given by the Berry phase acquired by the state around a small loop. Then, we numerically integrate the Berry curvature to obtain the Chern number. For a more detailed description, see Ref. 20.

The model systems used in the present work are the checkerboard lattices with 4×3 and 5×3 unit cells at filling $\nu = \frac{1}{3}$, i.e. $N_p = 4$ particles on $N_s = 4 \times 3 \times 2 = 24$ lattice sites and $N_p = 5$ particles on $N_s = 5 \times 3 \times 2 = 30$ lattice sites, respectively. We perturb the system by varying up to five of the nearest-neighbor hopping amplitudes, i.e. setting $t_{jk} \rightarrow s$ for some of the hopping amplitudes and $t_{jk} \rightarrow t$ to all others in the first term

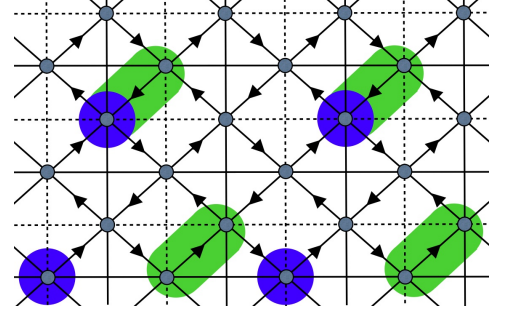


FIG. 1. (Color online) The checkerboard lattice with 4×3 unit cells that is used in the computations. The arrows indicate the direction where the sign of the complex phase ϕ_{jk} in the nearest-neighbor hopping is positive. In the next-nearest-neighbor hopping, dashed and solid lines have opposite signs. In addition, there is a next-next-nearest-neighbor hopping not drawn in the figure for clarity. The green ovals and the blue circles indicate the positions of the impurity hoppings and impurity potentials, respectively.

of the Hamiltonian (1), or by inserting up to five local potentials by adding terms of the form

$$H_j^{\text{pot}} = p n_j \quad (4)$$

to the Hamiltonian. Negative and positive values of p correspond to attractive and repulsive potentials, respectively. The locations of these impurities have been chosen such that they are evenly distributed in the lattice, as presented in Figure 1 for the 4×3 unit cell lattice.

To gain insight into the phase transitions caused by the impurities, we compute the spectrum of the one-body reduced density matrix (1-RDM)²¹ with elements

$$\rho_{ij} = \langle \Psi_0 | c_i^\dagger c_j | \Psi_0 \rangle, \quad (5)$$

where $|\Psi_0\rangle$ is the ground state. The 1-RDM eigenstates are called natural orbitals (NO). For trivial uncorrelated single Slater determinant states the eigenvalues of the 1-RDM have values 0 and 1, and for correlated states they fall somewhere in-between, indicating that the state cannot be fully described by single particle physics. The sum of the 1-RDM eigenvalues equals the particle number, and in a FQH state the nonzero eigenvalues are equal to the filling fraction. Thus, by computing the 1-RDM spectrum we obtain information about the quantity of correlations present, and furthermore, how the impurities bind particles from the correlated many-body state.

We solve the lowest eigenstates and energies by the exact diagonalization method in the full Hilbert space. We use the Lanczos algorithm to obtain the lowest eigenstates and eigenenergies of the Hamiltonian. In the Lanczos iteration, typically only the lowest eigenstate will be accurate enough, so to obtain the excited states, we run the algorithm multiple times, and shift up the eigenvalues of the states that have already been computed. The

shift is done by adding

$$H_m^{\text{shift}} = \lambda \sum_{i=0}^{m-1} |\Psi_i\rangle \langle \Psi_i| \quad (6)$$

to the Hamiltonian when computing the m th eigenstate $|\Psi_m\rangle$. This will increase the eigenvalues of the previously computed states by λ , so as long as λ is a large enough positive number, the next Lanczos iteration will converge to the m th eigenstate. Our implementation of the Lanczos algorithm runs fully on a graphics processor, programmed with the CUDA programming model²².

III. IMPURITIES

Previously, the effect of adding attractive local potentials to the checkerboard lattice has been discussed in Ref. 14. Phase transitions to a metallic state and a topologically trivial insulating phase were observed to take place with increasing strength of the potentials. We would like to conduct a more thorough study of the robustness of the FQHE state against different kinds of impurities, including a variable concentration of local potentials and variations in the hopping amplitudes between sites.

We detect the phase transitions caused by the impurities by computing the low energy and the 1-RDM spectra. The FQH phase is clearly identified by the threefold quasi-degenerate ground state manifold with a unit total Chern number, separated by a large gap from the higher energy states. Transitions from the topological FQH phase into a metallic phase are characterized by the collapse of the energy gap above the GSM. The insulating phase has one ground state that is separated from other states by a large gap in the whole (θ_1, θ_2) plane. It is also topologically trivial, indicated by the vanishing Chern number of the ground state.

The 1-RDM spectra can be used to corroborate the analysis: the localization of the particles onto the impurities leads to fully occupied natural orbitals, i.e. unit eigenvalues. In the highly correlated FQH phase, we observe non-integer eigenvalues whereas in the trivial insulator phase all nonzero eigenvalues are very close to unity.

Explicitly, we use the following criteria to determine the phase: the system is in the FQH phase if the GSM has a unit total Chern number and the energy gap above the GSM is larger than the width of the GSM, averaged over the twisted boundary conditions. If the ground state has a vanishing Chern number and its 1-RDM spectrum has as many eigenvalues larger than 0.95 as the particle number, the system is in the insulating phase. Otherwise, the system is in the metallic phase. These criteria are of course somewhat arbitrary, but fixing them allows us to compare the phases in systems of different sizes.

A. Impurity hoppings

We will now present our results for the 4×3 and 5×3 unit cell checkerboard lattices with added impurity hoppings. The energies of the ten lowest states at nearest-neighbor interaction strength $V = 3t$ are presented in Figure 2. They have been averaged over the twisted boundary conditions. The plots show the energies as a function of the impurity hopping strength s , and $n = 1, 2, 3, 4, 5$ indicates the number of impurity hoppings. The energy spectra on the left are from the 4×3 system with up to four impurity hoppings and on the right from the 5×3 system with up to five impurity hoppings. Additionally, in Figure 3, we present the 1-RDM spectra for the ground state of the 4×3 system at the points highlighted by the colored markers in Figure 2. The 1-RDM spectra for the 5×3 system are essentially identical.

With one modified hopping, i.e. $n = 1$, we observe an interesting energy spectrum for both system sizes. The ground state manifold and the gap to higher energy states seem to stay intact for $s > 1$. However, with $s < 1$ the gap closes with a small negative s but reopens with a larger negative s . For large negative values of s , there is a new threefold quasi-degenerate ground state manifold. The total Chern number of this new GSM is unity, so it seems that the FQH phase re-emerges at large negative s . The peculiar metallic phase in between has a total Chern number two so it could also be interpreted as two different FQH phases reorganizing as the impurity hopping changes sign.

The $n = 1$ 1-RDM spectrum in Figure 3 further supports the re-emergence of the FQH phase with a different GSM as seen in the corresponding energy plot. First of all, the 1-RDM spectrum of the unperturbed system at $s = 1$ is plotted in black. The first 12 eigenvalues are essentially zero, and they correspond to the states in the higher band in our non-interacting two-band model. The rest of the eigenvalues have non-integer values, as expected from the highly correlated $\nu = \frac{1}{3}$ FQH state. The 1-RDM spectra of the states with strong impurities, $s = 2$ and $s = -2$, are very similar. The shape reflects the division of the lattice into two distinct areas: because of the large hopping amplitude, a single electron is localized to the sites that are connected by the impurity, seen in the plot as the one almost fully occupied orbital. This localization, in turn, causes the occupation of the neighboring sites to decrease to avoid the cost of the repulsive NN interaction, indicated by the decreased occupancy in some NOs. In the remaining lattice, the rest of the particles form an FQH type phase, characterized by the non-integer part of the spectrum.

This interpretation is confirmed by looking at the natural orbital densities for each lattice site. In Figure 4, the fully occupied natural orbital is mostly localized on the two lattice sites connected by the impurity hopping, with some density on the neighboring sites and essentially zero density elsewhere. On the other hand, the

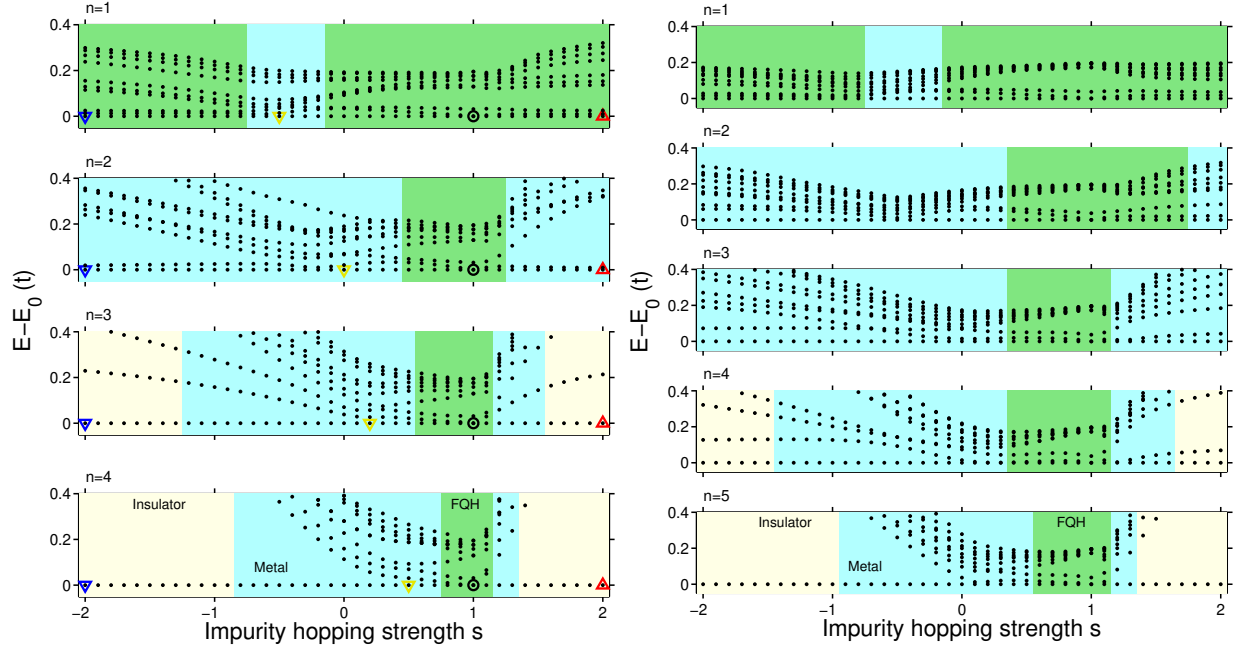


FIG. 2. (Color online) Ten lowest eigenenergies of the Hamiltonian in Eq. (2), averaged over the twisted boundary conditions. There are $n = 1, 2, 3, 4, 5$ added impurity hoppings at $V = 3t$ on 4×3 (left) and 5×3 (right) unit cell checkerboard lattices. The FQH, metallic and insulating phases are indicated by the different background colors, see the bottom panels.

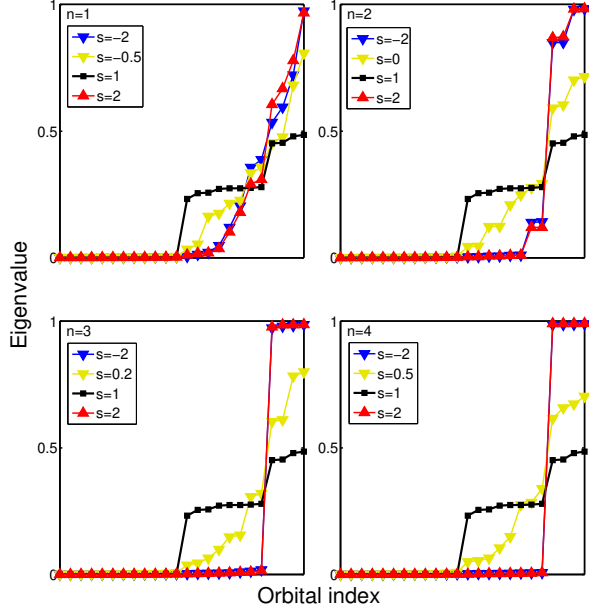


FIG. 3. (Color online) The spectra of the one-body reduced density matrices of the ground states at the highlighted points on the left hand side plots of Figure 2.

three next highest occupied NOs form a somewhat even density in the remaining lattice, with very little density at the impurity site or its nearest neighbors.

With two impurity hoppings, transitions to the metal-

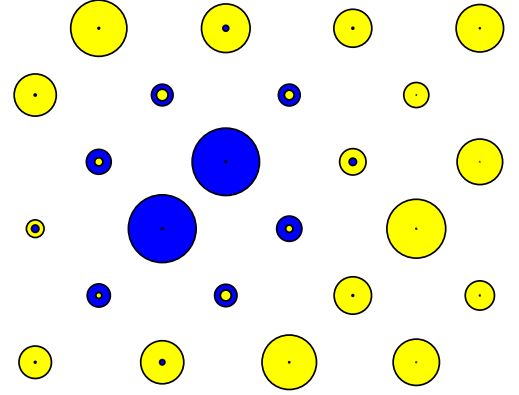


FIG. 4. (Color online) Natural orbital densities in the 4×3 unit cell checkerboard lattice with $n = 1$ impurity hopping at $s = -2$. The densities are indicated by the areas of the circles. The highest occupied natural orbital is plotted in blue, and the sum of the three next highest occupied natural orbitals is plotted in yellow.

lic phase occur for both negative and positive s . The 1-RDM spectra show two fully occupied NOs which are localized on the the two impurity hoppings. Again, the spectra for $s = 2$ and $s = -2$ are almost identical as the sign of the impurity hopping only affects the localized NOs, since the density of the other NOs vanishes on the sites connected by the impurities.

As the impurity density increases, the FQH region around the unperturbed system at $s = 1$ becomes narrower. With $n \geq 3$ for the 4×3 system and $n \geq 4$ for the 5×3 system, strong impurities cause a transition into the trivial insulating phase with one ground state separated from the others by a very large gap. This is because most or all particles have been localized on the impurities. The corresponding 1-RDM eigenvalues for $s = 2$ and $s = -2$ are all very close to zeros and ones, confirming that the ground state is almost fully uncorrelated.

B. Impurity potentials

Analogous results for the systems with up to five added impurity potentials are presented in Figures 5, 6 and 7. With one potential, we observe no phase transitions: the ground state manifold and the gap remain intact with both repulsive and attractive perturbations. Unlike with the single impurity hopping, there are no changes in the states in the GSM. The $n = 1$ 1-RDM spectra show that at $p = -2$ there is a fully occupied natural orbital, which is localized on the lattice site with the attractive potential.

As above with the impurity hoppings, the localization can be directly seen in the densities obtained from the most occupied NOs, presented in Figure 7. The fully occupied NO has most of its density in the lattice site with the attractive potential, while the three next highest occupied NOs are distributed elsewhere in the lattice, with a very small density near the impurity potential. Again, the conclusion is that the system is divided into the localized part near the impurity site and the FQH state elsewhere. Interestingly, there is a very smooth transition from the FQH state formed by four particles at $p = 0$ to the one formed by three particles at $p = -2$.

In the 4×3 system with two potentials, there are phase transitions to the metallic state with both attractive and repulsive impurities. Unlike in the case with impurity hoppings, there is a clear asymmetry between positive and negative values of p , clearly seen in the 1-RDM spectra. The strong attractive potentials at $p = -2$ have bound two particles to the impurities, seen in the two fully occupied NOs. On the other hand, the 1-RDM spectrum for the ground state with strong repulsive potentials at $p = 2$ is quite close to the unperturbed FQH ground state at $p = 0$. This is reasonable, since from the energy spectra one can see that the effect of the repulsive potentials is quite small: they only widen the GSM and make the gap smaller. In the 5×3 system, two repulsive potentials are not enough to break the FQH phase. This is most likely because the impurity concentration is smaller than in the 4×3 lattice, which results in the gap being more robust.

In the smaller system with three and four potentials, there is a quick phase transition into the metallic phase and onto the insulating phase with attractive potentials, while repulsive potentials only induce a transition to the

metallic phase. Again, in the larger system the FQH phase seems to be more resilient against repulsive potentials, as the gap above the GSM stays open with larger positive p than in the 4×3 system. However, with attractive potentials, we observe the same transition to the insulating phase through the metallic phase.

The cases with equal numbers of attractive impurity potentials and particles, i.e. $n = 4$ in the 4×3 system and $n = 5$ in the 5×3 system with negative p , correspond to the one studied in Ref. 14. Qualitatively, our results agree: there are two phase transitions, one from the FQH to the metallic phase, and another from the metallic phase to the insulating phase. We can clearly identify these phases in the corresponding 1-RDM spectra. There are quantitative distinctions, probably due to differences in system size and the location of the impurity potentials.

C. Finite size scaling

In the previous sections, we have presented results for two system sizes with 4×3 and 5×3 unit cells, respectively. The results are in qualitative agreement: the FQH state is robust against individual impurities and the FQH region becomes narrower with increasing concentration of impurities. The insulating phase is only obtained for strong impurity hoppings or strong attractive potentials when the impurity concentration is close to the filling fraction. To perform a rudimentary finite size scaling, we have also done computations on a 6×3 unit cell lattice with $N_p = 6$ particles.

The results in Figure 8 demonstrate the robustness of the FQH phase as a function of the lattice size for both low and high number of impurities. In Figure 8a, we plot the energy gap above the GSM divided by the width of the GSM with a single impurity hopping at strength $s = \pm 2$ and a single attractive potential with strength $p = \pm 2$. Note that here the impurity density decreases as the system becomes larger. At the thermodynamic limit, one would expect the FQH phase in the case of an individual local impurity. Unfortunately, we are only able to increase one of the dimensions in the system size because of the size limitation of the exact diagonalization method and the fact that the number of unit cells needs to be divisible by three to be able to support a $\nu = \frac{1}{3}$ FQH phase. Thus, properly extrapolating to the 2D thermodynamic limit is beyond the scope of this study. In Figure 8b, we plot the width of the FQH phase region in the presence of impurity hoppings and potentials, such that the number of impurities is equal to the number of particles. Here, the impurity density stays constant. Despite the thermodynamic limit being out of reach, it seems plausible that the remarkable robustness of the FQH phase extends also to larger systems.

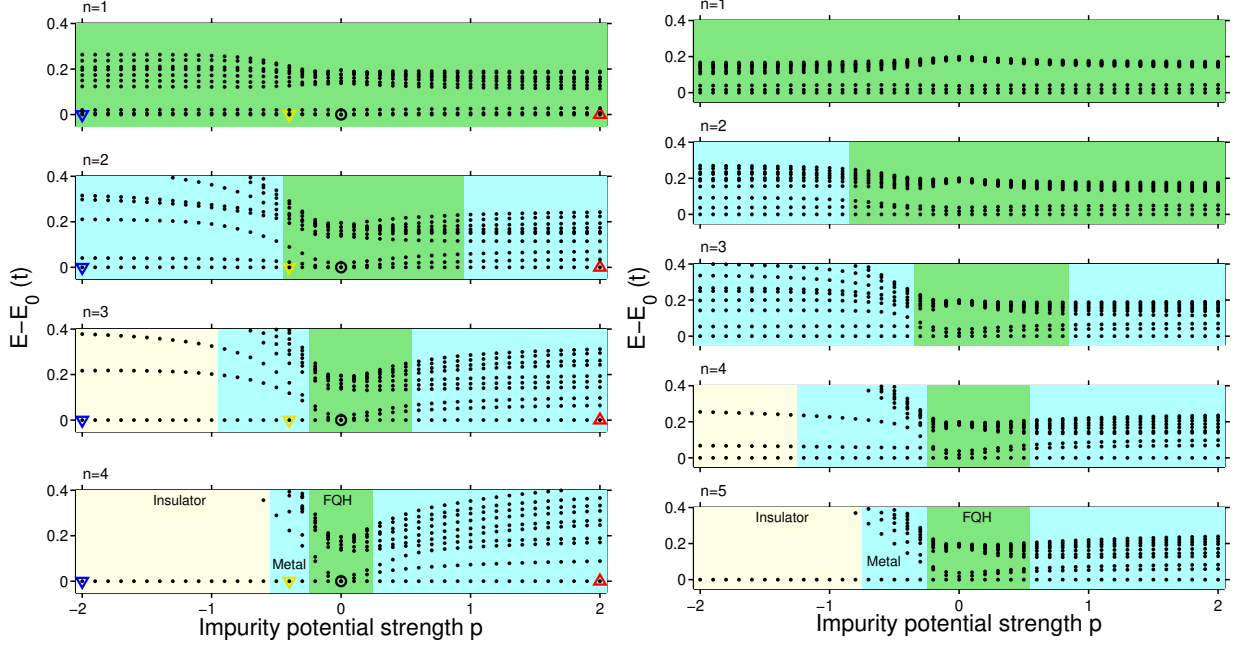


FIG. 5. (Color online) Ten lowest eigenenergies of the Hamiltonian in Eq. (2), averaged over the twisted boundary conditions. There are $n = 1, 2, 3, 4, 5$ added impurity potentials at $V = 3t$ on 4×3 (left) and 5×3 (right) unit cell checkerboard lattices. The FQH, metallic and insulating phases are indicated by the different background colors, see the bottom panels.

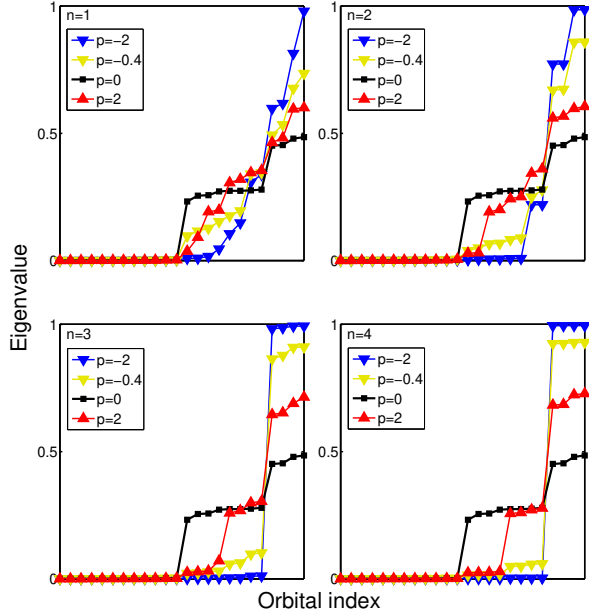


FIG. 6. (Color online) The spectra of the one-body reduced density matrices of the ground states at the highlighted points on the left hand side plots of Figure 5.

IV. LANDAU LEVEL MIXING

A feature in the 1-RDM spectra is the fact that in all cases the twelve lowest eigenvalues are nearly zero,

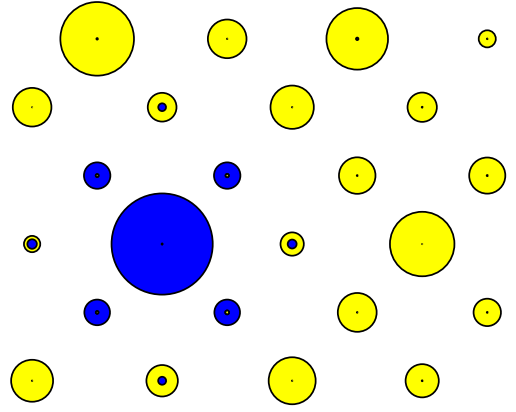


FIG. 7. (Color online) Natural orbital densities in the 4×3 unit cell checkerboard lattice with $n = 1$ impurity potential at $p = -2$. The densities are indicated by the areas of the circles. The highest occupied orbital is plotted in blue, and the sum of the three next highest occupied natural orbitals is plotted in yellow.

indicating vanishing occupancy of half of the natural orbitals. In the two-band checkerboard model, the flat energy band corresponds to the lowest Landau level (LLL) in the ordinary continuum quantum Hall effects. An explanation to these unoccupied natural orbitals is that they consist mostly of the excited single particle states lying above the nearly degenerate flatband states. This ob-

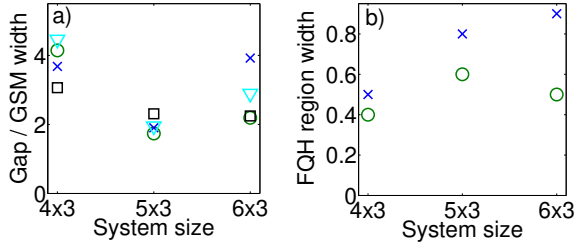


FIG. 8. (Color online) (a) The ratio of the energy gap above the GSM to the width of the GSM as a function of the system size in four cases: one impurity hopping at $s = -2$ (blue crosses) and $s = 2$ (teal triangles) and one impurity potential at $p = -2$ (green circles) and $p = 2$ (black squares). (b) The width of the FQH phase region with impurity hoppings (green circles) and impurity potentials (blue crosses) as a function of the system size. The number of the impurities is equal to the number of particles.

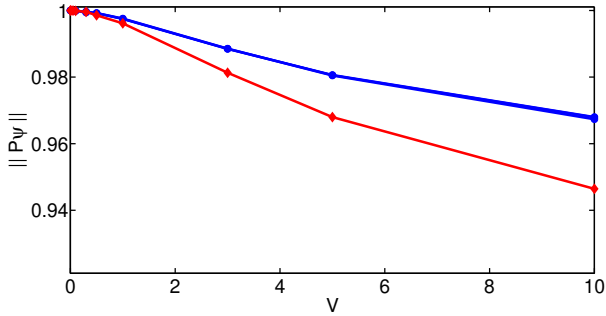


FIG. 9. (Color online) The norm of the three ground states (in blue) and the first excited state (in red) of the 4×3 unit cell checkerboard lattice after projecting them onto the LLL as a function of the nearest-neighbor interaction V , in units of t .

servation seems to imply very little mixing to the higher energy states even with strong impurities.

For example in Ref. 23, it has been conjectured that to obtain the FQH state, one should have the following hierarchy of energy scales:

$$b \ll V \ll \delta, \quad (7)$$

where b is the bandwidth of the flat band, V is the interaction and δ is the band gap. In the literature, computations have often been limited to the low-energy band by making it completely flat and projecting the states onto it, essentially making the band gap infinite^{7,8}. This allows for a smaller Hilbert space which makes computations easier and also ensures that the above criterion is fulfilled. However, it seems that it is not necessary to obey the hierarchy of Eq. (7) as our results were computed at $V = 3t$, which is certainly larger than the band gap in the checkerboard model. Moreover, in Refs. 24 and 25, much higher values of interaction have been used successfully.

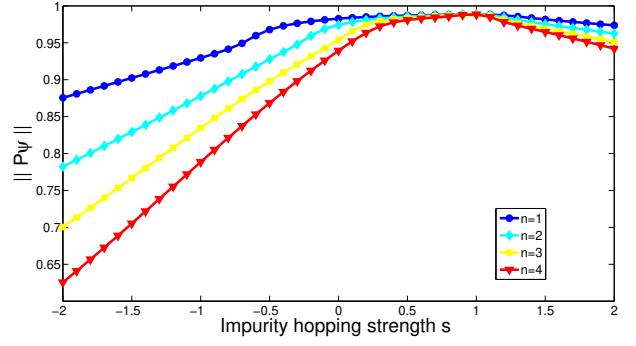


FIG. 10. (Color online) The norm of the ground states of the 4×3 unit cell checkerboard lattice with n impurity hoppings after projecting them onto the LLL as a function of the impurity strength.

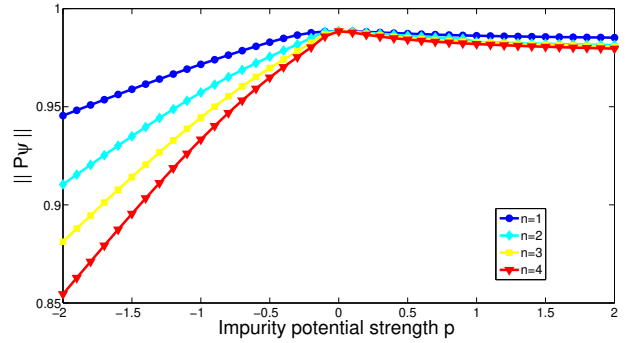


FIG. 11. (Color online) The norm of the ground states of the 4×3 unit cell checkerboard lattice with n impurity potentials after projecting them onto the LLL as a function of the impurity strength.

Since we have performed our calculations without any approximations to the Hilbert space, we can study how much mixing to higher states is caused by the interaction V and the various impurities. This is interesting from the point of view of a potential experimental realization of the model. Previously, mixing of bands with nonzero Chern numbers has been studied in a triangular lattice in Ref. 26.

We measure the extent of the mixing by projecting the computed ground states onto the lowest band with the projection operator

$$P = \sum_j |\phi_j\rangle \langle \phi_j|, \quad (8)$$

where $|\phi_j\rangle$ are the noninteracting Slater determinant states, formed from all combinations of the single particle states of the LLL. We can then measure the degree of mixing to higher states by computing the norm of the vector $P|\psi_0\rangle$. A unit norm indicates that the state is completely contained within the lowest Landau level.

In Figure 9, we present the norms of the three quasi-degenerate ground states and the first excited state as a function of the nearest-neighbor interaction V . We see

that even for much larger interaction strengths than the gap, which is on the order of t , there is very little mixing to the higher states. There is practically no difference between the three ground states, while the first excited state mixes slightly more.

To see whether the impurities cause mixing, we have also performed the projection onto the lowest band on the ground states of the perturbed systems. The norms of the resulting vectors are presented in Figure 10 (impurity hoppings) and Figure 11 (impurity potentials). The system is very robust against a single impurity hopping or potential, indicated by large norms even for strong perturbations. With increasing number of impurities, the mixing to the higher band is increased. However, it seems that there is little correlation between the norm of the projected vector and the phases obtained from the energy and 1-RDM spectra. All in all, even with many strong impurities, the ground states still mostly reside in the space formed by the states in the lowest Landau level.

V. CONCLUSIONS

In conclusion, we have performed an exact diagonalization calculation on the checkerboard lattice model with added impurities in the form of multiple modified nearest neighbor hoppings and local potentials. We computed the low energy spectra as well as the spectra of the one-body reduced density matrices of the ground states to identify the quantum phase transitions from the $\nu = \frac{1}{3}$ fractional quantum Hall phase into a metallic phase and a topologically trivial insulating phase.

The FQH state was found to be very robust against single impurities of both kind, as expected of a topological

state that should be stable against local perturbations. Increasing the number of impurities caused a transition to the metallic state. When the number of impurity hoppings was close to the particle number, a transition to the trivial insulating state was observed with both positive and negative hopping amplitudes. On the other hand, only attractive potentials were able to induce the same transition and the FQH phase was overall more robust against repulsive potentials.

Common to both impurity types, the FQH region became narrower with increasing impurity density. Qualitatively similar results were obtained for three finite systems of 4×3 , 5×3 and 6×3 unit cells with 4, 5 and 6 particles and up to 4, 5 and 6 impurities, respectively. Based on our results, it seems that the $\nu = \frac{1}{3}$ FQH phase in the checkerboard lattice can withstand both very strong isolated impurities and a high density of weaker impurities, which is a reassuring result for any attempts at an experimental realization of the system.

We also showed that very little mixing between the single particle bands is induced by the nearest neighbor interaction or impurities. This validates the approximation used in many previous studies of restricting the Hilbert space to only the states in the lowest Landau level.

ACKNOWLEDGMENTS

T.S acknowledges financial support from the Finnish Doctoral Programme in Computational Sciences FICS. This research has also been supported by the Academy of Finland through its Centres of Excellence Program (project no. 251748). We acknowledge the computational resources provided by Aalto Science-IT project and Finland's IT Center for Science (CSC).

-
- ¹ Z. Ezawa, *Quantum Hall Effects: Field Theoretical Approach and Related Topics* (World Scientific Publishing Company, Incorporated, 2000).
 - ² X. Wen, *Quantum Field Theory of Many-Body Systems: From the Origin of Sound to an Origin of Light and Electrons*, Oxford Graduate Texts (OUP Oxford, 2004).
 - ³ F. D. M. Haldane, Phys. Rev. Lett. **61**, 2015 (1988).
 - ⁴ E. Tang, J.-W. Mei, and X.-G. Wen, Phys. Rev. Lett. **106**, 236802 (2011).
 - ⁵ T. Neupert, L. Santos, C. Chamon, and C. Mudry, Phys. Rev. Lett. **106**, 236804 (2011).
 - ⁶ K. Sun, Z. Gu, H. Katsura, and S. Das Sarma, Phys. Rev. Lett. **106**, 236803 (2011).
 - ⁷ Y.-L. Wu, B. A. Bernevig, and N. Regnault, Phys. Rev. B **85**, 075116 (2012).
 - ⁸ B. A. Bernevig and N. Regnault, Phys. Rev. B **85**, 075128 (2012).
 - ⁹ N. Regnault and B. A. Bernevig, Phys. Rev. X **1**, 021014 (2011).
 - ¹⁰ T. Scaffidi and G. Möller, Phys. Rev. Lett. **109**, 246805 (2012).
 - ¹¹ D. J. Thouless, M. Kohmoto, M. P. Nightingale, and M. den Nijs, Phys. Rev. Lett. **49**, 405 (1982).
 - ¹² D. N. Sheng, Z.-C. Gu, K. Sun, and L. Sheng, Nat. Commun. **2** (2011).
 - ¹³ D. N. Sheng, X. Wan, E. H. Rezayi, K. Yang, R. N. Bhatt, and F. D. M. Haldane, Phys. Rev. Lett. **90**, 256802 (2003).
 - ¹⁴ S. Yang, K. Sun, and S. Das Sarma, Phys. Rev. B **85**, 205124 (2012).
 - ¹⁵ X. G. Wen and Q. Niu, Phys. Rev. B **41**, 9377 (1990).
 - ¹⁶ D. Arovas, J. R. Schrieffer, and F. Wilczek, Phys. Rev. Lett. **53**, 722 (1984).
 - ¹⁷ X. G. Wen, Phys. Rev. Lett. **66**, 802 (1991).
 - ¹⁸ E. Kapit, P. Ginsparg, and E. Mueller, Phys. Rev. Lett. **108**, 066802 (2012).
 - ¹⁹ B. Juliá-Díaz, T. Graß, N. Barberán, and M. Lewenstein, New J. Phys. **14**, 055003 (2012).
 - ²⁰ R. Resta, EPJ B **79**, 121 (2011).
 - ²¹ A. J. Coleman, Rev. Mod. Phys. **35**, 668 (1963).
 - ²² T. Siro and A. Harju, Comp. Phys. Comm. **183**, 1884 (2012).

- ²³ S. A. Parameswaran, R. Roy, and S. L. Sondhi, C. R. Phys. **14**, 816 (2013).
- ²⁴ S. Kourtis, T. Neupert, C. Chamon, and C. Mudry, Phys. Rev. Lett. **112**, 126806 (2014).
- ²⁵ S. Kourtis, J. W. F. Venderbos, and M. Daghofer, Phys. Rev. B **86**, 235118 (2012).
- ²⁶ S. Kourtis and M. Daghofer, arxiv:1305.6948 (2013).